Carbon Energy

WILEY

CARBON ENERGY

RESEARCH ARTICLE OPEN ACCESS

Energy-Efficient Induction Carbonization: Tailoring Pore Structures in Hard Carbon Anodes Toward Enhanced Electrochemical Performance

Yanghao Jin[1] | Mengwei Sun[2] | Ziyi Shi[1] | Dumindu Pasan Siriwardena Thanaweera Achchige[3] | Huiting Liu[4,5] | Hanmin Yang[1] | Yaprak Subasi[3] | Ritambhara Gond[3] | Yazhe Wang[1] | Habtom Desta Asfaw[3] | Yun Tian[2] | Manuel Baumann[4] | Marcel Weil[4,6] | YongGang Yao[7] | Haiping Yang[8] | Reza Younesi[3] | Pär G. Jönsson[1] | Weihong Yang[1] | Tong Han[1,8]

[1]Department of Material Science and Engineering, KTH Royal Institute of Technology, Stockholm, Sweden | [2]Interdisciplinary Research Center for Sustainable Energy Science and Engineering (IRC4SE2), School of Chemical Engineering, Zhengzhou University, Zhengzhou, Henan, China | [3]Department of Chemistry—Ångström Laboratory, Uppsala University, Uppsala, Sweden | [4]Institute for Technology Assessment and Systems Analysis (ITAS), Karlsruhe Institute of Technology, Karlsruhe, Germany | [5]Institute of Technical Thermodynamics, RWTH Aachen University, Aachen, Germany | [6]Helmholtz Institute Ulm (HIU), Ulm, Germany | [7]State Key Laboratory of Materials Processing and Die & Mould Technology, School of Materials Science and engineering, Huazhong University of Science and Technology, Wuhan, Hubei, China | [8]State Key Laboratory of Coal Combustion, School of Energy and Power Engineering, Huazhong University of Science and Technology, Wuhan, Hubei, China

Correspondence: Tong Han (tong.han@nordicbiographite.com)

Received: 14 October 2025 | **Revised:** 26 January 2026 | **Accepted:** 12 March 2026

Funding: VINNOVA, Grant/Award Number: 2021-03735; Deutsche Forschungsgemeinschaft, Grant/Award Number: 390874152

ABSTRACT

Hard carbon (HC) is currently the predominant anode material for sodium-ion batteries; however, its practical application is still limited by insufficient initial Coulombic efficiency (ICE) and plateau capacity. Meanwhile, conventional HC production relies on energy-intensive carbonization processes with considerable carbon emissions. Here, an induction heating carbonization strategy is developed for extruded biocarbon columns derived from biomass-based biochar and bio-oil, enabling simultaneous enhancement of electrochemical performance and production sustainability. Bio-oil combined with high-pressure extrusion suppresses open pores, whereas induction heating generates localized eddy currents and concentrated Joule heating that accelerate carbon rearrangement and promote closed pore formation. As a result, the closed-to-open pore volume ratio increases from 0.32 to 85.18, leading to improved ICE (95.0% vs. 84.4%) and plateau capacity ratio (77.6% vs. 64.7%) relative to conventional carbonized HC. Life-cycle assessment further indicates an approximately 35% reduction in global warming potential. Overall, this work presents an energy-efficient, low-emission route for producing high-performance HC anodes.

1 | Introduction

Sodium-ion batteries (SIBs) are widely regarded as a promising alternative to lithium-ion batteries (LIBs) for large-scale energy storage applications. They offer potential advantages in terms of costs, usage of abundant sodium resources, and excellent performance at low temperatures [1]. Thus, they could be applied in a wide range of applications in the future [2]. Among the various reported anode materials for SIBs, hard carbon (HC) has been extensively investigated and remains the sole material used in commercial SIBs [3, 4].

Despite its potential, the widespread application of HC still faces many challenges in both production and performance [5, 6].

Yanghao Jin and Mengwei Sun contributed equally to this work.

In SIBs, an HC anode typically has both a slope region and a plateau region during charging and discharging. The slope capacity is attributed to the adsorption behavior of sodium-ion at surface defects, whereas the plateau capacity primarily relates to sodium-ion intercalation in the graphitic layers and filling in closed pores [7, 8]. Due to the inherent porosity of raw materials such as biomass and charcoal, HC has certain specific surface areas and open pore volumes, which provide abundant sites for sodium-ion adsorption [9]. However, these porous structures also promote electrolyte decomposition, leading to the significant formation of a solid electrolyte interphase (SEI) layer during initial charge/discharge cycle. This extensive SEI formation contributes to substantial electrochemical irreversibility, resulting in suboptimal initial Coulombic efficiency (ICE) and limiting the practical application of HC in SIBs [10, 11]. Literature reports indicate that the ICE values of HC materials produced without modification approaches are typically below 90%, with the majority not exceeding 80% [12]. Various strategies have been used to reduce the surface area to address this issue, including surface engineering via chemical vapor deposition (CVD) [13], raw materials' pre-treatment [14], and high-pressure compression [15]. Despite these efforts, the ICE values for most HC materials are typically lower than 90% (Supporting Information S1: Table S1), which remains significantly lower than that of graphite anodes in lithium-ion batteries (LIBs) [16].

Furthermore, the enhancement of the ICE would inevitably result in diminished adsorption behavior of sodium-ion and a corresponding decrease in slope capacity. Consequently, the low-voltage plateau capacity, which arises from the interlayer embedding and/or closed pore filling of sodium-ion, becomes the primary contributor to the higher energy density of HC anodes for SIBs. Numerous efforts have been devoted toward enlarging the volume of closed pores to maximize the plateau capacity of HC [17], and it is widely accepted that high-temperature carbonization facilitates the formation of closed pores [18]. However, high-temperature processing is inherently energy-intensive. More importantly, the current carbonization process predominantly utilizes indirect heating, wherein heat is externally supplied and transferred to the material [19, 20]. This approach requires the furnace to operate at temperatures significantly higher than the target temperature to ensure adequate inward heat flux [20, 21]. Consequently, the resulting energy inefficiencies not only limit the formation of closed pores but also lead to substantial emissions [4, 22, 23].

It is a significant challenge to enhance the ICE of HC to match that of graphite anodes in LIBs while simultaneously generating a substantial number of closed pores to boost plateau capacity [24]. In this study, we propose a scalable and sustainable approach for HC production involving induction heating carbonization (IC) of biocarbon columns formed by compressing a composite consisting of biocarbon and bio-oil, as depicted in Figure 1A and Supporting Information S1: Figure S1. By inducing eddy currents within the biocarbon columns, this method significantly promotes open pore closure and massive closed pore formation. Compared to HC derived from conventional heating carbonization (CC) methods, the result HC products show a significant inversion of the closed-to-open pore volume ratio (85.18 vs. 0.32), leading to substantial improvements in ICE (above 95% vs. 84.4%) and reversible capacity (280 mAh/g compared to 198 mAh/g at the 2nd cycle), particularly in plateau capacity and its ratio (77.6% vs. 64.7%, Figure 1B). Simultaneously, the ICE value, closed pore volume, and the corresponding plateau capacity ratio of our HC products surpass those reported in the literature (Figure 1C,D) [9, 18, 25–43]. The present study offers a novel approach for the preparation of HC, addressing the inherent issue of low ICE and low plateau capacity, potentially driving the production of HC toward an efficient and sustainable direction.

2 | Results and Discussion

2.1 | Hard Carbon Synthesis Through Efficient Induction Heating Carbonization

Induction heating carbonization directly generates heat through eddy currents within the biocarbon, representing an innovative and highly energy-efficient heating technique. To elucidate these advantages, we utilized Finite Element Method to simulate the thermal fields within the furnace during the carbonization process for both CC and IC. The detailed model is provided in Supporting Information S1: Section 3.1.

The thermal field simulations reveal that CC results in a declining temperature gradient from the wall to the sample surface (Figure 2A). Achieving a target temperature of 1580 K for HC requires heat source temperatures exceeding 1800 K, which imposes significant energy demand. Conversely, as depicted in Figure 2B, IC concentrates the heat directly within HC samples, leading to higher temperatures compared to the surrounding environment in a short time. Correspondingly, IC shows instantaneous heating efficiency (on average $> 80\%$ vs. $< 40\%$) superior to CC methods (Supporting Information S1: Figure S2). During the insulation stage at 1580 K, the two methods show markedly different heat transfer dynamics (Figure 2C). In IC, heat flows from the sample outward to the environment, whereas in CC, it transfers from the environment into the sample. This distinction means that all the energy utilized in IC is directed toward heating the sample, which accounts for its high heating efficiency [45]. Meanwhile, IC has a heat flux that is almost 10 times higher than that of CC. This suggests that IC concentrates a greater amount of energy on the sample, ensuring rapid energy supply for structural transformation and reducing the overall carbonization time required for HC production. Consequently, as shown in Supporting Information S1: Figure S3, the calculated overall carbonization energy demand for IC (202.7 kJ/g) is nearly three times lower than the energy required by CC (504.6 kJ/g) under laboratory-scale production.

The present study further investigates the influence of the IC on HC structures. Commercially available biocarbon samples derived from sawdust (a mixture of pine and spruce) are utilized in this study, with detailed analysis provided in Supporting Information S1: Table S2. Specifically, four different HC samples (after bio-oil modification) are prepared by IC under varying conditions and named according to their specific preparation parameters, such as HC-3.59%-1000-3h (volatile content–carbonization temperature duration). For comparison, samples are also prepared using the CC method, for example, CC-HC-1300-3h. The detailed procedure is shown in the Supporting Information S1: Section 1.2.

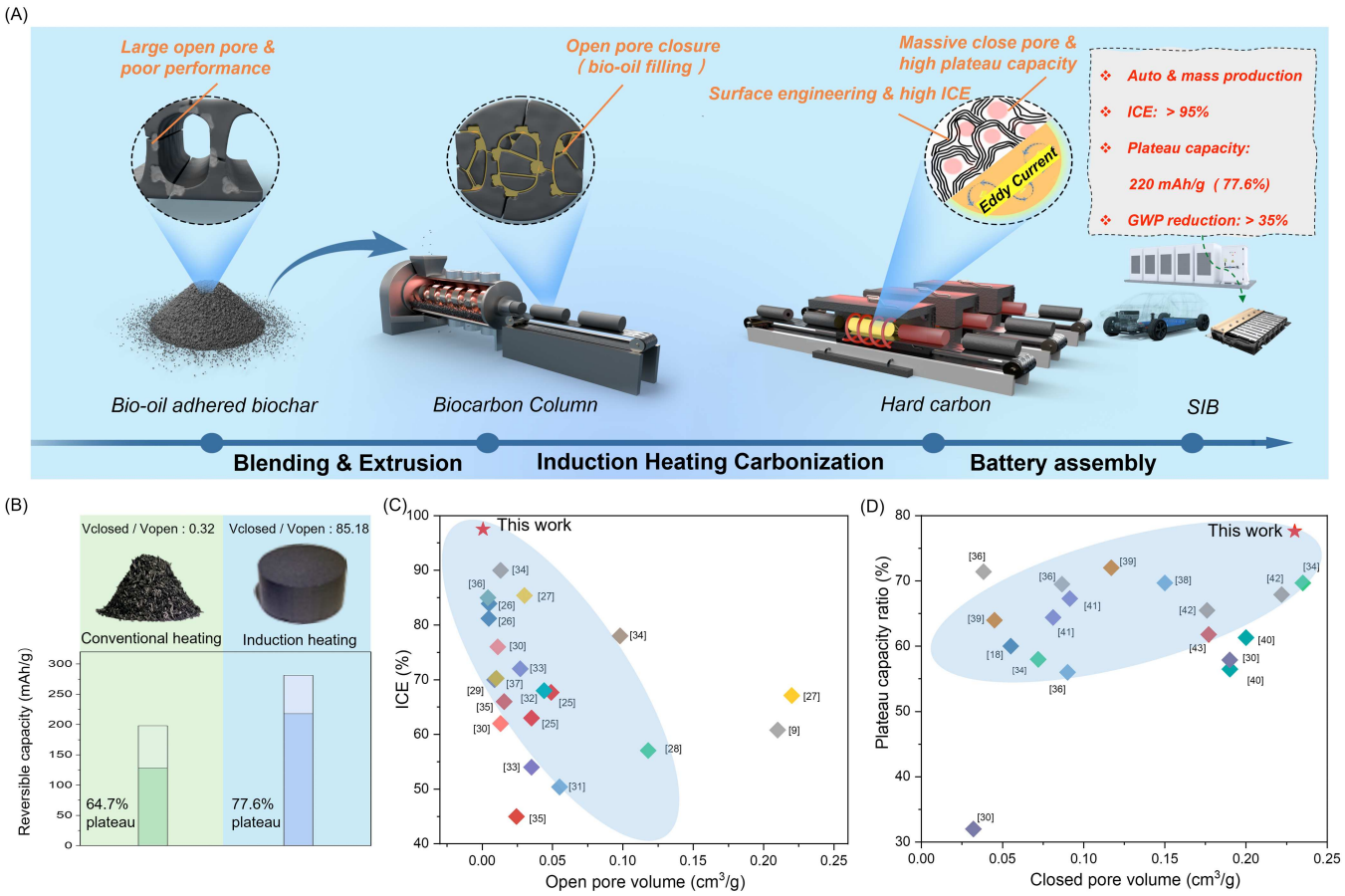

FIGURE 1 | Induction heating carbonization of extruded biocarbon. (A) Schematic figure of the proposed induction heating carbonization of extruded biocarbon. (B) Comparison between conventional and induction heating carbonization. Relationship between (C) ICE and open pore volume and (D) plateau capacity ratio and closed pore volume in the literature [9, 18, 25–43].

The micropore structure of HC is critical to its electrochemical performance. To evaluate the open pore structure of HCs, a CO_2 adsorption/desorption measurement is performed. The open pore volume of different HC samples is shown in Figure 2D and Supporting Information S1: Table S3, and the corresponding adsorption/desorption isotherm lines are provided in Supporting Information S1: Figure S4. CC-HC-1300-3h shows a significantly higher open pore volume of approximately 0.1763 cm^3/g. In contrast, HC samples prepared via IC consistently show extremely low open pore volumes, not exceeding 0.01 cm^3/g, with HC-13.79%-1300-1h showing a value of approximately 0.0027 cm^3/g. These values are nearly 80 times lower than those of CC-HC-1300-3h, highlighting the effectiveness of bio-oil modification combined with IC in promoting the closure of open pores.

Estimates of the closed pore volumes are obtained from the true density measurements (Supporting Information S1: Table S3) using graphite as a reference. Figure 2E shows the closed pore volumes of different samples. Similarly, HC samples prepared via IC show significantly higher closed pore volumes compared to those prepared using the CC method. Specifically, HC-3.59%-1300-3h and HC-13.79%-1300-1h show closed pore volumes (0.218 and 0.23 cm^3/g, respectively) that are nearly 4 times higher than that of CC-HC-1300-3h (0.058 cm^3/g). These findings demonstrate that the IC approach also offers unique advantages in promoting the formation of closed pores. As mentioned above, high-temperature carbonization facilitates the formation of closed pores [46]. Consequently, HC-3.59%-1300-3h and HC-13.79%-1300-1h also show significantly higher closed pore volumes in comparison with HC 3.59%-1000-3h and HC-13.79%-1000-1h.

X-ray diffraction (XRD) and Raman spectroscopy are performed, and the results are shown in Supporting Information S1: Figures S5 and S6. Figure 2F presents the corresponding I_D/I_G ratio versus d_{002} results for various samples. It is evident that an increase in carbonization temperature leads to enhanced ordering of carbon atoms (as indicated by a decrease in the I_D/I_G ratio) and reduced interlayer spacing (d_{002}), both of which are indicative of the temperature rise promoting the rearrangement of carbon atoms to form graphite-like layers. Compared with the CC-HC-1300-3h sample, both HC-3.59%-1300-3h and HC-13.79%-1300-1h show lower I_D/I_G ratios and d_{002}. This result is consistent with the energy analysis results, which concluded that IC concentrates a greater amount of energy on the sample, ensuring rapid energy supply for structural transformation (formation of curled graphite layers) and reducing the overall time required for HC production. Correspondingly, distinct curled graphite layers with abundant closed pores are clearly observable in the high-resolution transmission electron microscopy (TEM) image of HC-13.79%-1300-1h (Figure 2G), whereas no obvious curled graphite layers or closed pores are evident in that of CC-HC-1300-3h

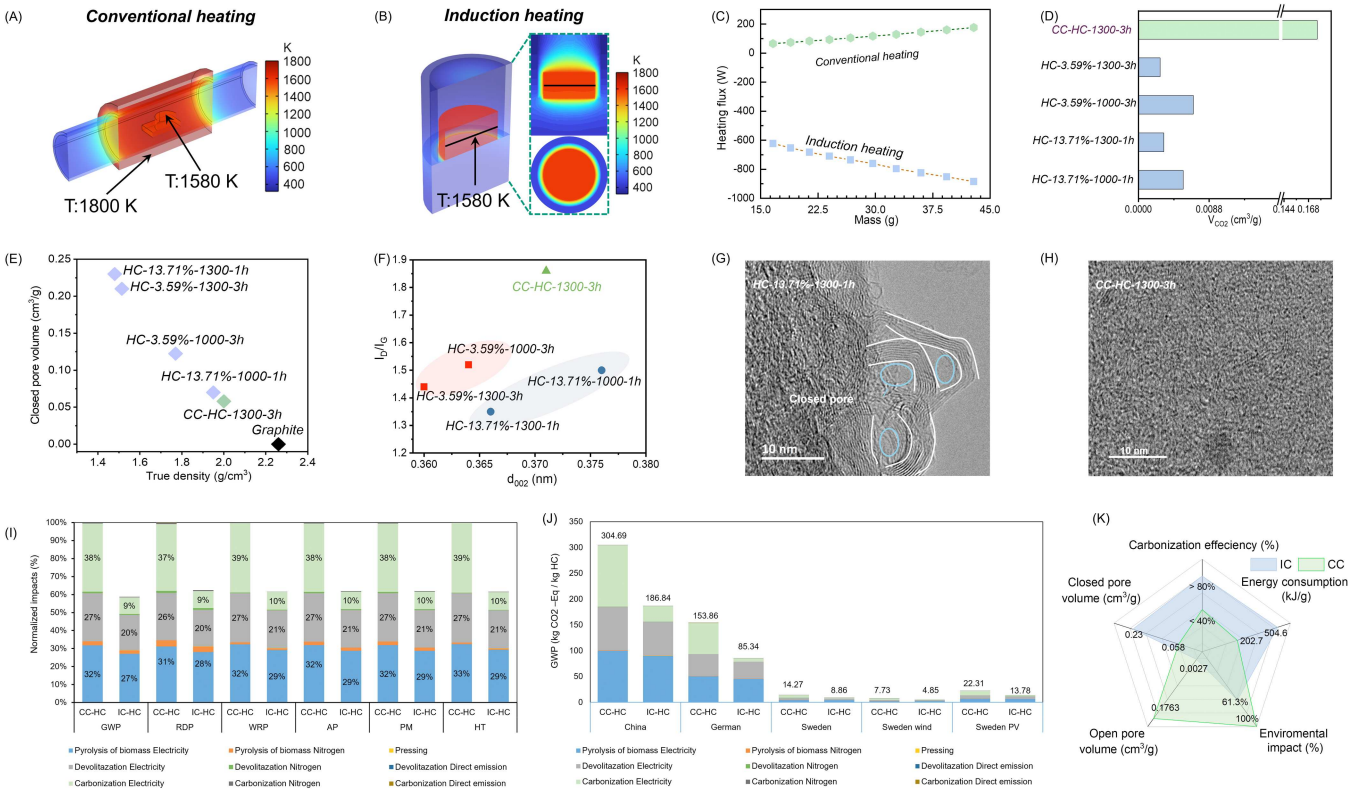

FIGURE 2 | Process energy analysis and HC products characterization: temperature distribution in (A) a conventional heating furnace after 10 min and (B) an induction heating furnace after 1 min. (C) Heating flux of different carbonization methods during the isothermal period. (D) Open pore volume of HC samples. (E) Closed pore volume versus the true density of HC samples. (F) Relationship between I_D/I_G and d_{002} of HCs samples. High-resolution TEM image of (G) HC-13.71%-1300-1h and (H) CC-HC-1300-3h. (I) Environmental impact of CH-HC and IC-HC (relative amount) based on a Swedish electricity and supply chain. (J) GWP of CC-HC and IC-HC under different scenarios; Reproduced with permission: Copyright 2026, Elsevier [44]. (K) Comparison between IC and CC approaches.

(Figure 2H). This closed pore–rich microstructure is expected to contribute to a higher plateau capacity during charging and discharging by providing additional sodium-ion storage sites.

To further evaluate the environmental impact of different carbonization methods, a cradle-to-gate life-cycle assessment (LCA) is performed based on a comprehensive process model covering the entire production line from raw biomass to the final HC product. The functional unit is defined as 1 kg of produced HC anode material, and the modeling details are presented in the Supporting Information S1: Section 3.2. Inventory data for the two methods (CC-HC and IC-HC) are included in the Supporting Information S1: Table S4 and S5.

The mass and energy balance calculations are based on experimental data combined with COMSOL simulation results, compensating for the lack of industrial reference data. Supporting Information S1: Figure S7 illustrates the mass balance throughout the IC-HC process model, revealing that approximately 3.72 kg of raw biomass is required to produce 1 kg of HC. To enable a comparative analysis, the synthesis pathway of CC-HC is modeled with the same background system (identical supply chain of raw materials and energy). Results indicate that IC-HC achieves a reduction of over 35% in all considered environmental impact categories, as illustrated in Figure 2I. This highlights the significant benefits of the IC-HC approach in mitigating environmental burdens when compared to conventional methods of CC-HC.

A region-specific comparison of global warming potential (GWP) between two carbonization methods is conducted based on the emission factors for different electricity mixtures for 2022, which changed significantly in recent years and will continue to change in the coming years. Significantly, the GWP heavily depends on the energy resources utilized in different regions, as shown in Figure 2J. For nations heavily reliant on fossil fuel–generated electricity, such as China [47], the GWP of the IC-HC approach is estimated at 186.84 $kg_{CO2\text{-}equivalents}/kg_{HC}$. In German, more than 50% electricity is generate form renewable source in 2023 [48], which leads to a significantly lower GWP of 85.34 $kg_{CO2\text{-}equivalents}/kg_{HC}$. Conversely, countries like Sweden, with a higher ratio (about 90% [49]) of renewable energy sources, can achieve a remarkably low GWP of 8.86 $kg_{CO2\text{-}equivalents}/kg_{HC}$. This finding underscores the importance of renewable energy integration for the innovative IC approach in ensuring a cleaner supply chain and sustainable development for future battery systems.

In summary, compared with CC (Figure 2K), IC offers an efficient, low-energy, and sustainable route for HC synthesis, enabling the production of optimized HC with suppressed open pores and abundant closed pore structures.

2.2 | Electrochemical Performance of HC Product

The electrochemical performance of HC samples produced via IC is initially assessed using SIB half-cells assembled with an active material mass loading of 1–3 mg/cm^2. Figure 3A presents the 1st cycle charge–discharge capacity and corresponding ICE values of cells assembled with various HC samples prepared by induction heating carbonization. It is evident that HC anodes show an ICE exceeding 89% and a reversible capacity greater than 240 mAh/g, both of which are significantly higher than that of HC anode (84.4%) prepared using the CC method.

Notably, the optimized sample, HC-13.71%-1300-1h, achieves the highest ICE of 97.5%, which is comparable to that of graphite anodes in LIBs and far surpasses the reported literature values [50]. The IC approach offers a simplified method for significantly enhancing the ICE of HC anodes in SIBs, addressing one of the primary bottlenecks to their commercial application [51]. Figure 3B compares the differential capacity (d_Q/d_V) versus cell voltage plots of the HC-13.71%-1300-1h anode and the CC-HC-1300-3h anode. The CC-HC-1300-3h anode shows an obvious redox peak at around 0.5 V, which is not observed for the HC-13.71%-1300-1h anode. According to the literature, the redox peak at around 0.5 V is attributed to the decomposition of the electrolyte to form the SEI layer [52, 53], indicating that almost no SEI layer formed on the HC-13.71%-1300-1h anode. Moreover, the curve of the HC-13.71%-1300-1h anode approaches zero between 0.1 and 0.5 V, implying that the proportion of sodium-ion adsorption at the carbon layer edges and defects is very low. Cyclic voltammetry (CV) scans of the CC-HC-1300-3h anode and the HC-13.71%-1300-1h anode, shown in Figure 3C, further elucidate the differences in SEI formation. A significant irreversible peak is observed for the CC-HC-1300-3h anode between the 1st and 2nd scans, indicating substantial SEI layer formation. However, the curves of the 1st and 2nd scans nearly overlap, with only minor differences, suggesting that either an extremely thin or negligible SEI layer is formed. Additionally, the mild and wide voltage range reductions of the HC-13.71%-1300-1h anode may facilitate the gradual formation of a dense SEI layer with advanced

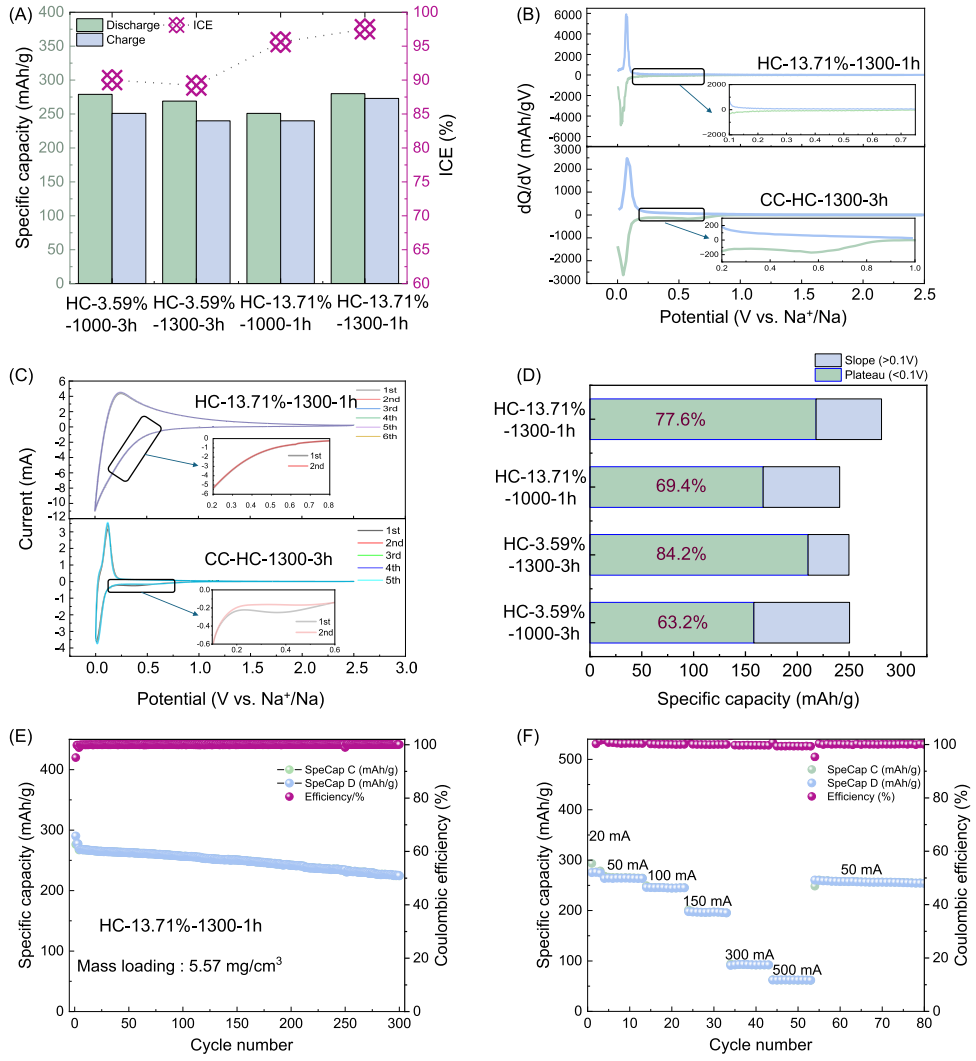

FIGURE 3 | Electrochemical performance of HCs. (A) Initial charging/discharging capacity and ICE of inducted carbonization HC samples at a current of 20 mA/g, (B) dQ/dV plots, and (C) cyclic voltammetry (CV) performance of HC-13.71%-1300-1h and CC-HC-1300-3h. (D) Specific capacity (mAh/g) and corresponding plateau region (< 0.1 V) ratio of the 2nd discharge of different HC samples. (E) Cycle performance of HC-13.71%-1300-1h-HMLE. (F) Rate performance of HC-13.71%-1300-1h-HMLE from 20 mA/g to 500 mA/g.

layer-by-layer structures, which could protect electrode materials more effectively [54]. A more detailed description of the SEI formation is provided in Supporting Information S1: Supplementary Discussion 1.

Figure 3D compares the reversible capacity and the plateau capacity ratio of different HC anodes prepared via IC. The plateau capacity ratio of all HC anodes exceeds 63%. Notably, the HC-3.59%-1300-3h and HC-13.71%-1300-1h anodes demonstrate significantly higher plateau capacities and corresponding ratios compared to the HC-3.59%-1000-3h and HC-13.71%-1000-1h anodes. Moreover, these values are also considerably superior to those of the CC-HC-1300-3h anode, suggesting that the IC approach markedly enhances both the plateau capacity and the corresponding ratio. Specifically, the optimized HC-13.71%-1300-1h anode shows approximately 85 mAh/g in capacity enhancement and a 12.9% increase in the ratio compared to the CC-HC-1300-3h anode. This improvement is a major contributor to the overall increase in reversible capacity.

High mass loading electrode (HMLE) enhances the active material content within individual cells, leading to reduced production costs and higher energy densities [54–56]. To evaluate the commercial potential of the optimized HC-13.71%-1300-1h sample, we fabricated HC-HMLE with an increased active material coating (over 5.4 mg/cm^2) using 1 mol $NaPF_6$ in diglyme as the electrolyte, and assessed their electrochemical performance as half-cells. As depicted in Figure 3E, the cell demonstrates a reversible capacity of approximately 280 mAh/g and an ICE exceeding 95%. The consistent electrochemical behavior of the charging/discharging curve indicates that the HC-13.71%-1300-1h sample can sustain its exceptional performance under high mass loading conditions. Additionally, the specific capacity demonstrates a retention rate of approximately 82% after around 300 cycles (Supporting Information S1: Figure S8), which is comparable to findings reported in the literature (Supporting Information S1: Table S1) [57, 58]. The rate capacity of the HC sample is tested to assess the reversible capacity at a high charging rate. As plotted in Figure 3E, the specific reversible capacity values of 266, 245, 197, 93, and 62 mAh/g are observed at charging rates of 0.2, 0.4, 0.8, 1.6, and 2 C (1 C = 250 mA/g), respectively. Finally, the HC-HMLE has been utilized as an anode coupling with a commercial Prussian white cathode to prepare pouch-type full-cell batteries. Notably, the full-cell can deliver a high discharge capacity of 96 mAh/g (based on the mass of the cathode), with an output voltage of 3.1 V, as shown in Supporting Information S1: Figure S9.

To further reveal the structural effects on sodium-ion storage behaviors, in situ Raman spectroscopy and in situ XRD are utilized to comparatively investigate the electrochemical behaviors of two HC materials: a predominantly closed pore structure (HC-13.71%-1300-1h) and a conventionally prepared HC with larger interlayer spacing and lower closed pore density (CC-HC-1300-3h).

The corresponding in situ Raman spectra for both materials are presented in Figure 4A. For CC-HC-1300-3h, upon decreasing the discharge voltage from 2 V to 0.01 V, the G band shifted from 1600 cm^{-1} to 1575 cm^{-1}, whereas the D band gradually diminished and disappeared at around 0.3 V. This shift can be attributed to the insertion of sodium-ion into the pseudo-graphitic structure, weakening and stretching the C–C bonds, leading to a redshift in the G peak and the disappearance of the D peak [59]. Conversely, the G band in HC-13.71%-1300-1h showed no significant shift throughout the charge–discharge cycle, indicating that sodium-ion storage primarily occurred through pore filling rather than intercalation [60].

As shown in Figure 4B, for CC-HC-1300-3h anodes, the (002) peak remains stable at approximately 22.5° within the voltage range from 3 V to 0.4 V. Upon further discharge below 0.1 V, the (002) peak shifted from 22.5° to 22°, indicating an increase in interlayer spacing due to sodium-ion diffusion into the carbon layers. In contrast, HC-13.71%-1300-1h shows a stable (002) peak at approximately 21.5° during the entire charge–discharge cycle, indicating that sodium-ion intercalation into the carbon layers is limited [61, 62]. This stability results from sodium-ion storage in closed pores, which does not affect the interlayer spacing [60]. Additionally, upon discharge below 0.1 V, a peak corresponding to Na metal appeared at around 29°, confirming sodium-ion storage through pore filling [63, 64]. This result aligns with the in situ Raman findings, confirming that sodium storage in HC-13.71%-1300-1h predominantly occurs in closed pores.

The observed differences in sodium-ion storage mechanisms are primarily due to structural variations resulting from the two heating methods. CC-HC-1300-3h, prepared by conventional heating, possesses a larger interlayer spacing and minimal closed pores, favoring intercalation. Conversely, HC-13.71%-1300-1h, produced by induction heating, has a smaller interlayer spacing, which limits intercalation but provides more closed pores for filling. This interpretation aligns with the dQ/dV voltage plots; the CC-HC-1300-3h anode shows a pronounced redox peak at around ~0.5 V, which is absent for HC-13.71%-1300-1h. Therefore, the three-stage adsorption–intercalation–closed pore filling mechanism is highly suitable for the sodium storage mechanism of the HC products in this study [65], as depicted in Figure 4C. A more detailed discussion of HC-13.71%-1300-1h electrochemical performance is provided in Supporting Information S1: Supplementary Discussion 1.

2.3 | Mechanism Study of HC Prepared by Induction Heating Carbonization

Based on the characterization and electrochemical results, the effect of IC on HC and its performance is investigated. Initially, a mini-review is conducted (Supporting Information S1: Supplementary Discussion 2) to clarify the key properties of HC products that determine their electrochemical performance. It is redefined that the SSA/open pore volume of HC is essential for its ICE value, and the interlayer distance and closed pore volume of HC are essential for its reversible capacity. More specifically, closed pores play a crucial role in contributing to the low-voltage plateau capacity. Figure 5A summarizes the relationship between the ICE value and the open volumes of the HC samples prepared at 1300°C in this study, as well as those reported in the literature. The results further confirm that a relatively low open pore volume is essential for achieving a high ICE value. Additionally, another series of samples were also fabricated by blending bio-oil with biocarbon and then subjected to high-pressure compression and carbonization using the CC method. These samples, named as CC-BHC-1300-3h,

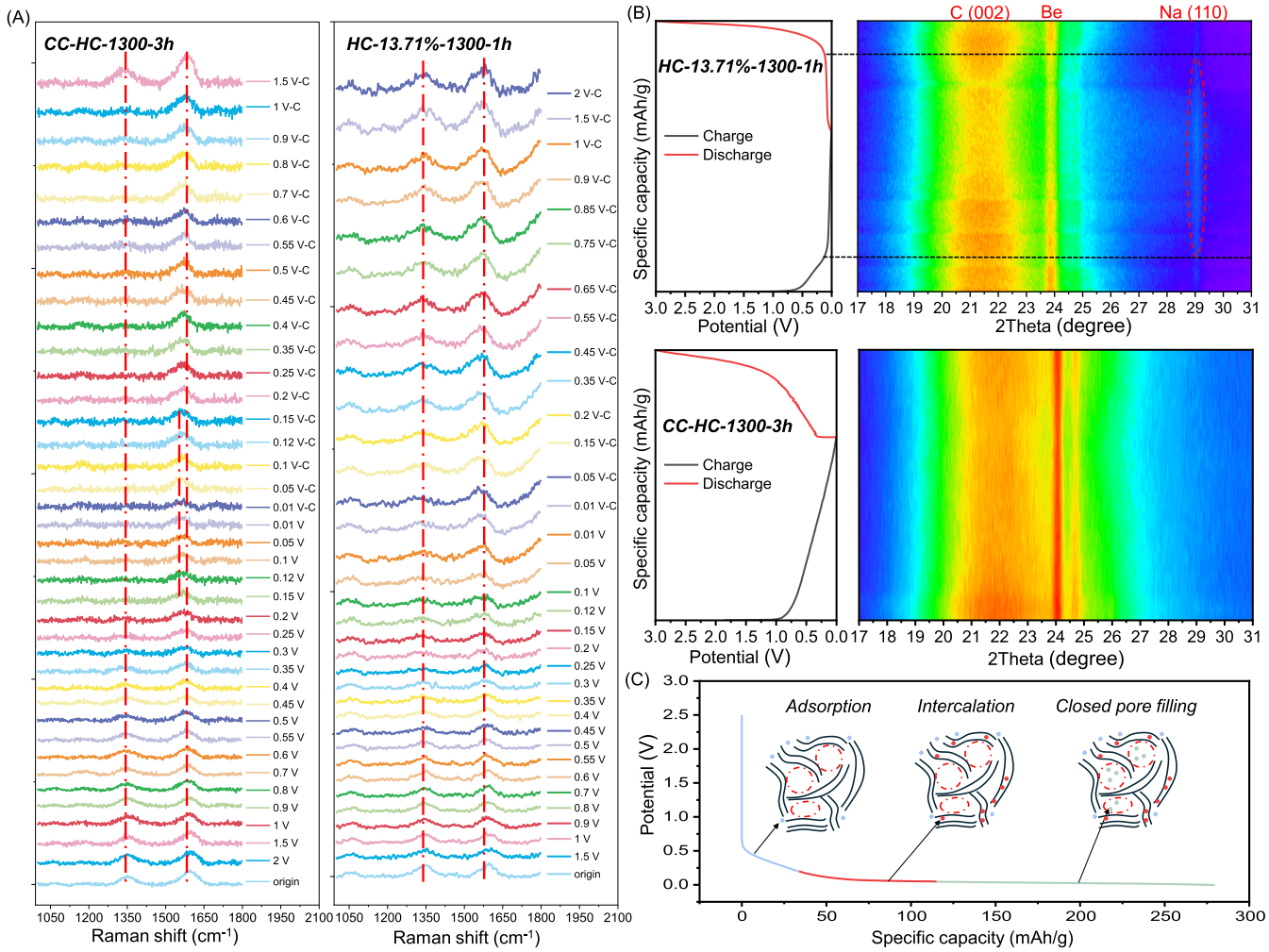

FIGURE 4 | Mechanistic study of sodium-ion storage in HCs. (A) In situ Raman spectra of HCs. (B) In situ XRD patterns with the potential–time curve of HCs. (C) Sodium-ion storage mechanism in HC.

were reported in our previous study [44]. The relationship between the ICE value and the open volumes of the CC-HC-1300-3h sample and the CC-BHC-1300-3h sample is also presented in Figure 5A. CC-BHC-1300-3h, HC-3.59%-1300-3h, and HC-3.59%-1000-3h all show markedly higher ICE values (> 89%) than CC-HC-1300-3h (~84%), consistent with their substantially lower open pore volumes. Moreover, the ICE values of CC-BHC-1300-3h and HC-3.59%-1300-3h are remarkably close, and the open pore volumes of both samples fall within a consistently low range (< 0.011 cm^3/g). These results indicate that the addition of bio-oil, combined with subsequent high-pressure compression, can significantly reduce the open pore volume regardless of the heating method, thereby substantially increasing the ICE value of the HC anodes. However, for HC samples with high volatile content, an ultra-high ICE is observed despite similar open pore volumes, indicating the potential effect of IC and volatile contents on the ICE value.

The underlying mechanism is further inspected. As shown in Supporting Information S1: Figure S10, the working effect of bio-oil can be regarded as a surface engineering agent, which is filled into the open pores during its mixture with biocarbon and high-pressure compression. After the carbonization process, thickened carbon layers are formed, leading to the significant closure effect of open pores and an increase in ICE. A detailed explanation is provided in Supporting Information S1: Supplementary Discussion 3 and our previous paper [44].

Furthermore, bio-oil also serves as a binder for shaping the biocarbon. In this study, the determination of the bio-oil/biocarbon ratio is deliberated, which is presented in Supporting Information S1: Supplementary Discussion 4. However, due to limitations in the shaping process, the bio-oil to biocarbon ratio is fixed at 30:70 to ensure the reliable formation of biocarbon columns suitable for IC. A systematic investigation of the influence of bio-oil content on HC structure will be conducted in future work, following further optimization of the shaping process.

Figure 5B presents the closed pore volume, plateau capacity, and their ratios for HC samples derived from IC at 1300°C (i.e., HC-13.71%-1300-1h and HC-3.59%-1300-3h) and those derived from CC at 1300°C (i.e., CC-HC-1300-3h and CC-BHC-1300-3h). Specifically, the closed pore volume of HC-13.71%-1300-1h (0.230 cm^3/g) and HC-3.59%-1300-3h (0.218 cm^3/g) is more than three times higher than that of CC-BHC-1300-3h (0.070 cm^3/g), which is similar to that of CC-HC-1300-3h (0.058 cm^3/g). Consequently, the plateau capacity of HC-13.71%-1300-1h and HC-3.59%-1300-3h is significantly enhanced compared to that of

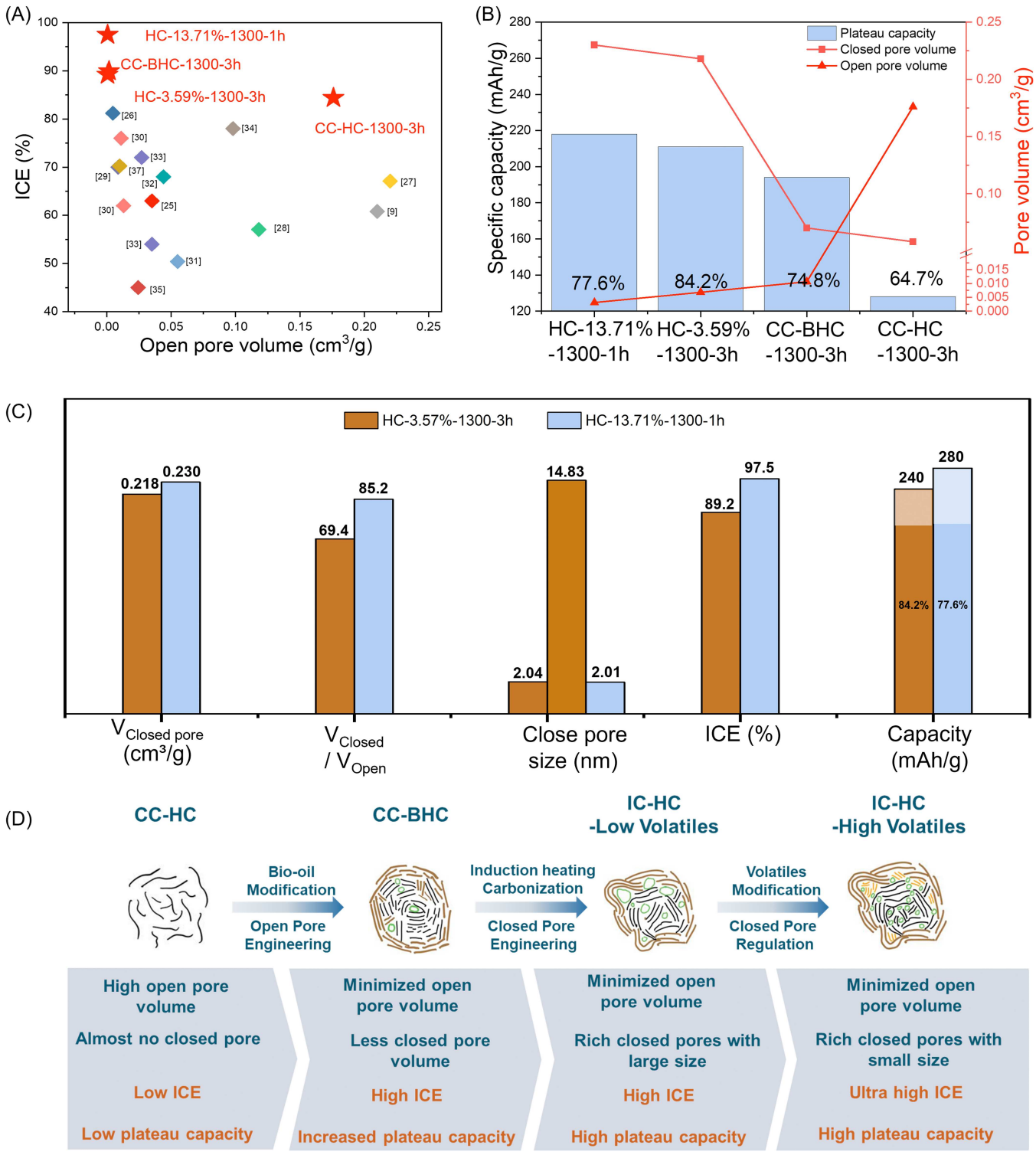

FIGURE 5 | Mechanistic study of HCs. (A) Relationship of ICE and open pore volume of HC samples. (B) Closed pore volume, open pore volume, and plateau capacity of HC samples. (C) Comparison of HC-3.57%-1300-3h and HC-13.71%-1300-1h. (D) Overall mechanism of the induction heating carbonization approach.

CC-BHC-1300-3h and CC-HC-1300-3h. These findings indicate that the IC is highly effective in promoting closed pore formation, thereby significantly increasing the plateau capacity. Moreover, elongated curled graphite layers are only detected for IC-HC, as depicted in the TEM images (Figure 2H and Supporting Information S1: Figure S11–S13). As further illustrated in Supporting Information S1: Figure S14, the working mechanism of the induction heating can be summarized as follows: Induction heating generates eddy currents within the HC under an alternating magnetic field. These eddy currents serve not only as localized sources of Joule heating, enabling rapid graphitic rearrangement, but also promote the preferential alignment of carbon layers into elongated and curled graphite-like structures, which in turn facilitates the formation

of closed pores. A detailed elaboration is presented in Supporting Information S1: Supplementary Discussion 5.

Compared with CC-HC-1300-3h, CC-BHC-1300-3h shows a significantly lower open pore volume while maintaining a similar closed pore volume (Figure 5B). This observation indicates that the closure of open pores is not necessarily linked to the formation of closed pores. In other words, reducing the open pore volume does not inherently result in more closed pores. This also suggests that the common assertion in the literature, which posits that closed pores are formed through the closure of open pores [66], lacks sufficient rigor. Although some studies have demonstrated the formation of closed pores through the sealing of activation-induced open pores [67], most closed pores originate from the growth of pre-existing enclosed domains [68] or from the curvature and rearrangement of graphite-like layers during high-temperature carbonization [46]. In the present work, this process is facilitated by induction heating, leading to IC-HC with a high closed pore volume.

A comprehensive comparison between HC-3.59%-1300-3h and HC-13.71%-1300-1h to elucidate the influence of the volatile content in the biocarbon samples is provided in Figure 5C. With increasing pyrolysis temperature, volatile contents are progressively released from the biocarbon, and part of them condense to form bio-oil [69]. However, unlike bio-oil, which mainly surrounds and modifies the surface of the biocarbon, the volatiles remain trapped within the biocarbon matrix during carbonization in this study. As a result, these retained volatiles play a distinct role in the structural transformation of HC during IC. As depicted in Figure 5C, the major difference caused by the different volatile content lies in the closed pore size, as shown in the small angel X-ray scattering (SAXS) images (Supporting Information S1: Figure S15). HC-3.59%-1300-3h shows two distinct closed pore sizes (around 2.04 nm and around 14.83 nm), whereas HC-13.71%-1300-1h only shows one closed pore size (around 2.01 nm), which corresponds to the TEM images (Supporting Information S1: Figure S13). As discussed above, the ICE of HC-13.71%-1300-1h is significantly higher than that of HC-3.59%-1300-3h. This difference can be partially attributed to a reduction in surface defects, as indicated by the decrease in the Raman I_D/I_G ratio from 1.44 to 1.35. Another potential explanation is that the large-sized pores located at the edges of the HC particles may still possess narrow pore mouths (< 0.35 nm) that are classified as closed in gas adsorption measurements but remain partially accessible to electrolyte species [7]. Such partial accessibility can promote electrolyte decomposition and SEI formation within these pores, thereby contributing to irreversible capacity loss [70]. Additionally, the closed pore size plays a crucial role in sodium storage behavior. Closed pores with a smaller sizes have higher sodium filling potentials, which reduces the risk of sodium metal plating at high current densities and thereby contributes to improved rate capability [71]. In summary, during carbonization, volatile contents are hindered from escaping the biocarbon matrix due to sealing and compression by bio-oil [72], resulting in more complete pore filling within the HC. Meanwhile, the decomposition and partial release of volatile contents leave behind internal free space [73] that acts as a template for subsequent closed pore formation under IC. A detailed elaboration is presented in Supporting Information S1: Supplementary Discussion 6.

The underlying mechanism of the overall approach is displayed in Figure 5D. The innovative induction heating carbonization method induces significant reconstruction of the pore structure in HC production. Compared to conventional heating carbonization methods, this approach combines an open pore closure effect, facilitated by the addition of a bio-oil surface engineering agent and high-pressure compression (Supporting Information S1: Supplementary Discussion 3, from CC-HC to CC-BHC), with a closed pore formation effect, enabled by the induction heating process (Supporting Information S1: Supplementary Discussion 5, from CC-BHC to IC-HC-low) and closed pore engineering with the aid of volatiles (Supporting Information S1: Supplementary Discussion 6, from IC-HC-low to IC-HC-high). As a result, the HC samples show a high closed pore volume with a smaller size while maintaining an extremely low open pore volume ($V_{Open\ pores} << V_{Closed\ pores}$; $V_{Closed\ pores}/V_{Open\ pores} > 85.18$), which is in stark contrast to HC samples prepared using the CC method ($V_{Open\ pores} >> V_{Closed\ pores}$; $V_{Closed\ pores}/V_{Open\ pores} \approx 0.32$). For HC samples prepared using bio-oil surface engineering agents and high-pressure compression but without induction heating (CC-BHC), both the open and closed pore volumes remain relatively low ($V_{Open\ pores} < V_{Closed\ pores}$; $V_{Closed\ pores}/V_{Open\ pores} \approx 6.56$). Consequently, the reconstruction of the pore structure leads to a substantial enhancement of electrochemical performance. HC samples prepared using the IC method demonstrate superior ICE, plateau capacity, and plateau capacity ratio compared to those prepared using the conventional heating carbonization method, surpassing values reported in the literature for HC materials (Supporting Information S1: Table S1) [74–86].

3 | Conclusion

This study presents an innovative induction heating carbonization and pore engineering strategy for HC production. The process is divided into two stages. In the first stage, an open pore closure effect is achieved by introducing a bio-oil surface engineering agent coupled with high-pressure compression, effectively sealing off the open pores. In the second stage, the formation of closed pores is facilitated by the eddy currents and concentrated heat generated by induction heating. As a result, the resulting HC samples show an exceptionally high closed pore volume while maintaining an extremely low open pore volume. This unique structure leads to enhanced electrochemical performance, with an ICE above 95% and a plateau capacity of up to 220 mAh/g. Moreover, the efficient induction heating carbonization approach substantially reduces the energy demand for HC production, contributing to a lower environmental footprint.

Acknowledgements

The supply of raw materials for the experiments by Envigas is greatly appreciated. The TEM test support by Cheuk-Wai Tai from ARTEMI is appreciated. The authors extend their gratitude to Shiyanjia Lab (www.shiyanjia.com) for providing assistance with the SAXS, true density, and CO_2 adsorption analysis. The financial support by VINNOVA-Swedish Innovation Agency via the project number 2021-03735 is highly appreciated. This work contributes also to the research performed at CELEST (Center for Electrochemical Energy Storage Ulm-Karlsruhe).

The authors Huiting Liu, Marcel Weil, and Manuel Baumann acknowledge the financial support provided by the German Research Foundation (DFG) under Project ID 390874152 (POLiS Cluster of Excellence, EXC 2154).

Conflicts of Interest

The authors declare no conflicts of interest.

References

1. R. Usiskin, Y. Lu, J. Popovic, et al., "Fundamentals, Status and Promise of Sodium-Based Batteries," *Nature Reviews Materials* 6, no. 11 (2021): 1020–1035.

2. I. Hasa, S. Mariyappan, D. Saurel, et al., "Challenges of Today for Na-Based Batteries of the Future: From Materials to Cell Metrics," *Journal of Power Sources* 482 (2021): 228872.

3. X. Dou, I. Hasa, D. Saurel, et al., "Hard Carbons for Sodium-Ion Batteries: Structure, Analysis, Sustainability, and Electrochemistry," *Materials Today* 23 (2019): 87–104.

4. H. Liu, M. Baumann, X. Dou, et al., "Tracing the Technology Development and Trends of Hard Carbon Anode Materials-A Market and Patent Analysis," *Journal of Energy Storage* 56 (2022): 105964.

5. H. Liu, Z. Xu, Z. Guo, et al., "A Life Cycle Assessment of Hard Carbon Anodes for Sodium-Ion Batteries," *Philosophical Transactions. Series A, Mathematical, Physical, and Engineering Sciences* 379, no. 2209 (2021): 20200340.

6. P. Bai, Y. He, P. Xiong, X. Zhao, K. Xu, and Y. Xu, "Long Cycle Life and High Rate Sodium-Ion Chemistry for Hard Carbon Anodes," *Energy Storage Materials* 13 (2018): 274–282.

7. W. Zhang, Y. Du, Y. Qiu, et al., "Closed-Pore Engineering in Hard Carbon for Sodium Ion Storage: Advances, Challenges and Future Horizons," *Advanced Energy Materials* 15, no. 44 (2025): e03884.

8. X. Chen, J. Tian, P. Li, et al., "An Overall Understanding of Sodium Storage Behaviors in Hard Carbons by an "Adsorption-Intercalation/Filling" Hybrid Mechanism," *Advanced Energy Materials* 12, no. 24 (2022): 2200886.

9. N. Sun, Z. Guan, Y. Liu, et al., "Extended "Adsorption–Insertion" Model: A New Insight Into the Sodium Storage Mechanism of Hard Carbons," *Advanced Energy Materials* 9, no. 32 (2019): 1901351.

10. J. Yang, X. Wang, W. Dai, et al., "From Micropores to Ultra-Micropores Inside Hard Carbon: Toward Enhanced Capacity in Room-/Low-Temperature Sodium-Ion Storage," *Nano-Micro Letters* 13 (2021): 98.

11. R. F. Susanti, S. Alvin, and J. Kim, "Toward High-Performance Hard Carbon as an Anode for Sodium-Ion Batteries: Demineralization of Biomass as a Critical Step," *Journal of Industrial and Engineering Chemistry* 91 (2020): 317–329.

12. Y. Jin, Z. Shi, T. Han, et al., "From Waste Biomass to Hard Carbon Anodes: Predicting the Relationship Between Biomass Processing Parameters and Performance of Hard Carbons in Sodium-Ion Batteries," *Processes* 11, no. 3 (2023): 764.

13. B. Karaman, H. Tonnoir, D. Huo, et al., "CVD-Coated Carbon Xerogels for Negative Electrodes of Na-Ion Batteries," *Carbon* 225 (2024): 119077.

14. Y. Wang, J. Lu, W. Dai, et al., "On the Practicability of the Solid-State Electrochemical Pre-Sodiation Technique on Hard Carbon Anodes for Sodium-Ion Batteries," *Advanced Functional Materials* 34 (2024): 2403841.

15. Y. Du, Y. Qiu, R. Zhuang, et al., "Superior Initial Coulombic Efficiency and Areal Capacity of Hard Carbon Anode Enabled by Graphite-Assisted Carbonization for Sodium-Ion Battery," *Carbon* 221 (2024): 118929.

16. C. Zhao, Z. Yang, X. Zhou, et al., "Recent Progress on Electrolyte Boosting Initial Coulombic Efficiency in Lithium-Ion Batteries," *Advanced Functional Materials* 34, no. 5 (2024): 2303457.

17. Q. Meng, Y. Lu, F. Ding, Q. Zhang, L. Chen, and Y.-S. Hu, "Tuning the Closed Pore Structure of Hard Carbons With the Highest Na Storage Capacity," *ACS Energy Letters* 4, no. 11 (2019): 2608–2612.

18. S. Zhou, Z. Tang, Z. Pan, et al., "Regulating Closed Pore Structure Enables Significantly Improved Sodium Storage for Hard Carbon Pyrolyzing at Relatively Low Temperature," *SusMat* 2 no. 3 (2022): 357–367.

19. F. Jabari, B. Mohammadi-ivatloo, M. B. Bannae Sharifian, and S. Nojavan, "Design and Robust Optimization of a Novel Industrial Continuous Heat Treatment Furnace," *Energy* 142 (2018): 896–910.

20. Y. Zhuo, C. Li, C. Wu, and Y. Shen, "A Combined Numerical and Experimental Approach to Study the Carbonization of Low-Rank Coal Ellipsoidal Briquettes," *Chemical Engineering Science* 204 (2019): 76–90.

21. S. T. Wismann, J. S. Engbæk, S. B. Vendelbo, et al., "Electrified Methane Reforming: A Compact Approach to Greener Industrial Hydrogen Production," *Science* 364, no. 6442 (2019): 756–759.

22. J. Q. F Equipment, "Annual Output of 100T 1500°C Hard Carbon Anode Material Pilot Carbonization Furnace," accessed March 10, 2023. http://qianjinly.com/product/html/?171.html.

23. J. F. Peters, A. Peña Cruz, and M. Weil, "Exploring the Economic Potential of Sodium-Ion Batteries," *Batteries* 5, no. 1 (2019): 10.

24. H. Zheng, J. Zeng, X. Wan, et al., "ICE Optimization Strategies of Hard Carbon Anode for Sodium-Ion Batteries: From the Perspective of Material Synthesis," *Materials Futures* 3, no. 3 (2024): 032102.

25. N. Sun, H. Liu, and B. Xu, "Facile Synthesis of High Performance Hard Carbon Anode Materials for Sodium Ion Batteries," *Journal of Materials Chemistry A* 3, no. 41 (2015): 20560–20566.

26. M. Dahbi, M. Kiso, K. Kubota, et al., "Synthesis of Hard Carbon From Argan Shells for Na-Ion Batteries," *Journal of Materials Chemistry A* 5, no. 20 (2017): 9917–9928.

27. T. Zhang, J. Mao, X. Liu, et al., "Pinecone Biomass-Derived Hard Carbon Anodes for High-Performance Sodium-Ion Batteries," *RSC Advances* 7, no. 66 (2017): 41504–41511.

28. X. Zhu, X. Jiang, X. Liu, L. Xiao, and Y. Cao, "A Green Route to Synthesize Low-Cost and High-Performance Hard Carbon as Promising Sodium-Ion Battery Anodes From Sorghum Stalk Waste," *Green Energy & Environment* 2, no. 3 (2017): 310–315.

29. N. Zhang, Q. Liu, W. Chen, et al., "High Capacity Hard Carbon Derived From Lotus Stem as Anode for Sodium Ion Batteries," *Journal of Power Sources* 378 (2018): 331–337.

30. Y. Li, Y. Lu, Q. Meng, et al., "Regulating Pore Structure of Hierarchical Porous Waste Cork-Derived Hard Carbon Anode for Enhanced Na Storage Performance," *Advanced Energy Materials* 9, no. 48 (2019): 1902852.

31. F. Wu, M. Zhang, Y. Bai, X. Wang, R. Dong, and C. Wu, "Lotus Seedpod-Derived Hard Carbon With Hierarchical Porous Structure as Stable Anode for Sodium-Ion Batteries," *ACS Applied Materials & Interfaces* 11, no. 13 (2019): 12554–12561.

32. M. Lu, Y. Huang, and C. Chen, "Cedarwood Bark-Derived Hard Carbon as an Anode for High-Performance Sodium-Ion Batteries," *Energy & Fuels* 34, no. 9 (2020): 11489–11497.

33. C. Chen, Y. Huang, Y. Zhu, et al., "Nonignorable Influence of Oxygen in Hard Carbon for Sodium Ion Storage," *ACS Sustainable Chemistry & Engineering* 8, no. 3 (2020): 1497–1506.

34. S. Zhou, Z. Tang, G. Jin, et al., "Understanding the Relationship of Closed Pore Structure in Biomass-Derived Hard Carbon With Cellulose Regulating Strategy," *Small* 20 (2024): 2407341.

35. X. Ji, Y. Wei, H. Yang, et al., "Extended Plateau Capacity of Hard Carbon Anode for High Energy Lithium-Ion Batteries," *Small* 20 (2024): 2402616.

36. Z. Tang, D. Jiang, Z. Fu, et al., "Regulating Pseudo-Graphitic Domain and Closed Pores to Facilitate Plateau Sodium Storage Capacity and Kinetics for Hard Carbon," *Small Methods* 8 (2024): 2400509.

37. Y. Qiu, G. Jiang, Y. Su, et al., "Hybrid Hard Carbon Framework Derived From Polystyrene Bearing Distinct Molecular Crosslinking for Enhanced Sodium Storage," *Carbon Energy* 6, no. 7 (2024): e479.

38. Y. Li, A. Vasileiadis, Q. Zhou, et al., "Origin of Fast Charging in Hard Carbon Anodes," *Nature Energy* 9, no. 2 (2024): 134–142.

39. Z. Zheng, S. Hu, W. Yin, et al., "CO_2-Etching Creates Abundant Closed Pores in Hard Carbon for High-Plateau-Capacity Sodium Storage," *Advanced Energy Materials* 14, no. 3 (2024): 2303064.

40. B. Wang, S. Zhang, X. Jia, et al., "Tailoring Closed Pore Structure in Phenolic Resin Derived Hard Carbon Enables Excellent Sodium Ion Storage," *Chemical Engineering Journal* 499 (2024): 156126.

41. L. Liu, Y. Lan, N. Li, F. Sun, and N. Zhou, "Heterogeneous Carbon Coated Resin-Based Hard Carbon Anode Material for High-Performance Sodium Ion Batteries," *Materials Today Communications* 40 (2024): 109854.

42. D. Sun, L. Zhao, P. Sun, et al., "Rationally Regulating Closed Pore Structures by Pitch Coating to Boost Sodium Storage Performance of Hard Carbon in Low-Voltage Platforms," *Advanced Functional Materials* 34 (2024): 2403642.

43. J. Huang, E. Li, B. Dai, et al., "Regulating the Active Hydroxyl Group of Starch: Revealing the Evolution of Hard Carbon Structure and Sodium Storage Behavior," *Carbon* 229 (2024): 119527.

44. Y. Jin, H. Liu, H. Yang, et al., "Development of Biomass Pyrolysis Bio-Oil as a Renewable Surface Engineering Agent for Bio-Based Hard Carbon Production," *Journal of Power Sources* 641 (2025): 236824.

45. O. Lucía, P. Maussion, E. J. Dede, and J. M. Burdío, "Induction Heating Technology and Its Applications: Past Developments, Current Technology, and Future Challenges," *IEEE Transactions on Industrial Electronics* 61, no. 5 (2013): 2509–2520.

46. Z. Tang, R. Zhang, H. Wang, et al., "Revealing the Closed Pore Formation of Waste Wood-Derived Hard Carbon for Advanced Sodium-Ion Battery," *Nature Communications* 14, no. 1 (2023): 6024.

47. P. Zou, Q. Chen, Y. Yu, Q. Xia, and C. Kang, "Electricity Markets Evolution With the Changing Generation Mix: An Empirical Analysis Based on China 2050 High Renewable Energy Penetration Roadmap," *Applied Energy* 185 (2017): 56–67.

48. F. Ise, "Public Net Electricity Generation 2023 in Germany: Renewables Cover the Majority of the Electricity Consumption for the First Time," accessed August 03, 2024. https://www.ise.fraunhofer.de/en/press-media/press-releases/2024/public-electricity-generation-2023-renewable-energies-cover-the-majority-of-german-electricity-consumption-for-the-first-time.html.

49. Statista, "Distribution of Electricity Generation in Sweden in 2022, by Source," accessed August 3, 2024. https://www.statista.com/statistics/1013726/share-of-electricity-production-in-sweden-by-source/.

50. Y. Yang, C. Wu, X. X. He, et al., "Boosting the Development of Hard Carbon for Sodium-Ion Batteries: Strategies to Optimize the Initial Coulombic Efficiency," *Advanced Functional Materials* 34, no. 5 (2024): 2302277.

51. M. Zhang, Y. Li, F. Wu, Y. Bai, and C. Wu, "Boost Sodium-Ion Batteries to Commercialization: Strategies to Enhance Initial Coulombic Efficiency of Hard Carbon Anode," *Nano Energy* 82 (2021): 105738.

52. M. Ma, H. Cai, C. Xu, et al., "Engineering Solid Electrolyte Interface at Nano-Scale for High-Performance Hard Carbon in Sodium-Ion Batteries," *Advanced Functional Materials* 31, no. 25 (2021): 2100278.

53. L. Xiao, Y. Cao, W. A. Henderson, et al., "Hard Carbon Nanoparticles as High-Capacity, High-Stability Anodic Materials for Na-Ion Batteries," *Nano Energy* 19 (2016): 279–288.

54. F. Wu, M. Liu, Y. Li, et al., "High-Mass-Loading Electrodes for Advanced Secondary Batteries and Supercapacitors," *Electrochemical Energy Reviews* 4 (2021): 382–446.

55. J. Welch, R. Mogensen, W. van Ekeren, H. Eriksson, A. J. Naylor, and R. Younesi, "Optimization of Sodium Bis (Oxalato) Borate (NaBOB) in Triethyl Phosphate (TEP) by Electrolyte Additives," *Journal of the Electrochemical Society* 169, no. 12 (2022): 120523.

56. A. Buckel, C. A. Hall, L. A. Ma, et al., "Importance of First Cycle Conditions on the Electrochemical Performance of Hard Carbon and Prussian White Based Sodium-Ion Batteries Using Fire Resistant," *Fluorine-Free Electrolyte. Batteries & Supercaps* 7, no 2 (2024): e202300533.

57. C. Zhao, Q. Wang, Y. Lu, B. Li, L. Chen, and Y.-S. Hu, "High-Temperature Treatment Induced Carbon Anode With Ultrahigh Na Storage Capacity at Low-Voltage Plateau," *Science bulletin* 63, no. 17 (2018): 1125–1129.

58. Z. Xu, J. Wang, Z. Guo, et al., "The Role of Hydrothermal Carbonization in Sustainable Sodium-Ion Battery Anodes," *Advanced Energy Materials* 12, no. 18 (2022): 2200208.

59. J. Okabe, Y. Fang, I. Moriguchi, and I. Furó, "Structural Evolution by Heat Treatment of Soft and Hard Carbons as Li Storage Materials: A Joint Nmr/Xrd/Tem/Raman Study," *Journal of Materials Chemistry A* 13, no. 19 (2025): 13962–13975.

60. Y. Xue, Y. Chen, Y. Liang, et al., "Substitution Index-Prediction Rules for Low-Potential Plateau of Hard Carbon Anodes in Sodium-Ion Batteries," *Advanced Materials* 37 (2025): 2417886.

61. J. Cui, W. Li, P. Su, et al., "Repair Surface Defects on Biomass Derived Hard Carbon Anodes With N-Doped Soft Carbon to Boost Performance for Sodium-Ion Batteries," *Advanced Energy Materials* 15 (2025): 2502082.

62. G. Zhang, H. Gao, D. Zhang, et al., "Transformative Catalytic Carbon Conversion Enabling Superior Graphitization and Nanopore Engineering in Hard Carbon Anodes for Sodium-Ion Batteries," *Carbon Energy* 7 (2025): e713.

63. A. Thomas, B. Pohle, J. Schultz, M. Hantusch, and D. Mikhailova, "NaOH Protective Layer for a Stable Sodium Metal Anode in Liquid Electrolytes," *Journal of Energy Storage* 77 (2024): 109900.

64. B. Zhang, C. M. Ghimbeu, C. Laberty, C. Vix-Guterl, and J. M. Tarascon, "Correlation Between Microstructure and Na Storage Behavior in Hard Carbon," *Advanced Energy Materials* 6, no. 1 (2016): 1501588.

65. T. Zhang, C. Li, F. Wang, et al., "Recent Advances in Carbon Anodes for Sodium-Ion Batteries," *Chemical Record* 22, no. 10 (2022): e202200083.

66. X. Chen, N. Sawut, K. Chen, et al., "Filling Carbon: A Microstructure-Engineered Hard Carbon for Efficient Alkali Metal Ion Storage," *Energy & Environmental Science* 16, no. 9 (2023): 4041–4053.

67. Y. Wang, W. Zhang, N. Sun, R. A. Soomro, G. Xu, and B. Xu, "Confined Carbonization of Pitch Assists the Closed Pore Engineering of Coal-Based Carbon for Superior Na-Ion Storage," *ACS Applied Materials & Interfaces* 17, no. 10 (2025): 15436–15445.

68. L. Yue, Y. Lei, Y. Niu, Y. Qi, and M. Xu, "Recent Advances of Pore Structure in Disordered Carbons for Sodium Storage: A Mini Review," *Chemical Record* 22, no. 10 (2022): e202200113.

69. X. Hu and M. Gholizadeh, "Progress of the Applications of Bio-Oil," *Renewable and Sustainable Energy Reviews* 134 (2020): 110124.

70. Y. Zhang, S.-W. Zhang, Y. Chu, et al., "Redefining Closed Pores in Carbons by Solvation Structures for Enhanced Sodium Storage," *Nature Communications* 16, no. 1 (2025): 3634.

71. S. Xiao, Y. J. Guo, H. X. Chen, et al., "Insight Into the Role of Closed-Pore Size on Rate Capability of Hard Carbon for Fast-Charging Sodium-Ion Batteries," *Advanced Materials* 37 (2025): 2501434.

72. Y. Chen, S. S. A. Syed-Hassan, Q. Li, et al., "Effects of Temperature and Aspect Ratio on Heterogeneity of the Biochar From Pyrolysis of Biomass Pellet," *Fuel Processing Technology* 235 (2022): 107366.

73. Z. Chen, J. Shen, W. Deng, et al., "Achieving Over 200 Wh Kg^{-1} Sodium-Ion Pouch Cell by Quantitative Engineering of Hard Carbon Pores," *National Science Review* 13, no. 3 (2026): nwaf566. https://doi.org/10.1093/nsr/nwaf566.

74. D. Cheng, Z. Li, M. Zhang, Z. Duan, J. Wang, and C. Wang, "Engineering Ultrathin Carbon Layer on Porous Hard Carbon Boosts Sodium Storage With High Initial Coulombic Efficiency," *ACS Nano* 17, no. 19 (2023): 19063–19075.

75. X. Li, J. Sun, W. Zhao, Y. Lai, X. Yu, and Y. Liu, "Intergrowth of Graphite-Like Crystals in Hard Carbon for Highly Reversible Na-Ion Storage," *Advanced Functional Materials* 32, no. 2 (2022): 2106980.

76. T. Xu, X. Qiu, X. Zhang, and Y. Xia, "Regulation of Surface Oxygen Functional Groups and Pore Structure of Bamboo-Derived Hard Carbon for Enhanced Sodium Storage Performance," *Chemical Engineering Journal* 452 (2023): 139514.

77. F. Xie, Z. Xu, Z. Guo, et al., "Achieving High Initial Coulombic Efficiency for Competent Na Storage by Microstructure Tailoring From Chiral Nematic Nanocrystalline Cellulose," *Carbon Energy* 4, no. 5 (2022): 914–923.

78. L. Xiao, H. Lu, Y. Fang, et al., "Low-Defect and Low-Porosity Hard Carbon With High Coulombic Efficiency and High Capacity for Practical Sodium Ion Battery Anode," *Advanced Energy Materials* 8, no. 20 (2018): 1703238.

79. X.-S. Wu, X.-L. Dong, B.-Y. Wang, J.-L. Xia, and W.-C. Li, "Revealing the Sodium Storage Behavior of Biomass-Derived Hard Carbon by Using Pure Lignin and Cellulose as Model Precursors," *Renewable Energy* 189 (2022): 630–638.

80. X. Zhao, Y. Ding, Q. Xu, X. Yu, Y. Liu, and H. Shen, "Low-Temperature Growth of Hard Carbon With Graphite Crystal for Sodium-Ion Storage With High Initial Coulombic Efficiency: A General Method," *Advanced Energy Materials* 9, no. 10 (2019): 1803648.

81. H. Zhang, W. Zhang, and F. Huang, "Graphene Inducing Graphitization: Towards a Hard Carbon Anode With Ultrahigh Initial Coulombic Efficiency for Sodium Storage," *Chemical Engineering Journal* 434 (2022): 134503.

82. J. Zhao, X. X. He, W. H. Lai, et al., "Catalytic Defect-Repairing Using Manganese Ions for Hard Carbon Anode With High-Capacity and High-Initial-Coulombic-Efficiency in Sodium-Ion Batteries," *Advanced Energy Materials* 13 (2023): 2300444.

83. X.-X. He, J.-H. Zhao, W.-H. Lai, et al., "Soft-Carbon-Coated, Free-Standing, Low-Defect, Hard-Carbon Anode to Achieve a 94% Initial Coulombic Efficiency for Sodium-Ion Batteries," *ACS Applied Materials & Interfaces* 13, no. 37 (2021): 44358–44368.

84. J. Wang, J. Zhao, X. He, Y. Qiao, L. Li, and S.-L. Chou, "Hard Carbon Derived From Hazelnut Shell With Facile HCl Treatment as High-Initial-Coulombic-Efficiency Anode for Sodium Ion Batteries," *Sustainable Materials and Technologies* 33 (2022): e00446.

85. B. H. Hou, Y. Y. Wang, Q. L. Ning, et al., "Self-Supporting, Flexible, Additive-Free, and Scalable Hard Carbon Paper Self-Interwoven by 1D Microbelts: Superb Room/Low-Temperature Sodium Storage and Working Mechanism," *Advanced Materials* 31, no. 40 (2019): 1903125.

86. F. Xie, Z. Xu, A. C. S. Jensen, et al., "Unveiling the Role of Hydrothermal Carbon Dots as Anodes in Sodium-Ion Batteries With Ultrahigh Initial Coulombic Efficiency," *Journal of Materials Chemistry A* 7, no. 48 (2019): 27567–27575.

Supporting Information

Additional supporting information can be found online in the Supporting Information section.
Supporting File: cey270243-sup-0001-Supplymentary_materials.docx.